

# Influence of Rotation on Pulsar Radiation Characteristics

Peyman Ahmadi <sup>1</sup> and R. T. Gangadhara <sup>2</sup>

*Indian Institute of Astrophysics, Bangalore-560034, India*

## ABSTRACT

We present a relativistic model for pulsar radio emission by including the effect of rotation on coherent curvature radiation by bunches. We find that rotation broadens the width of leading component compared to the width of trailing component. We estimate the component widths in the average pulse profiles of about 24 pulsars, and find that 19 of them have a broader leading component. We explain this difference in the component widths by using the nested cone emission geometry.

We estimate the effect of pulsar spin on the Stokes parameters, and find that the inclination between the rotation and magnetic axes can introduce an asymmetry in the circular polarization of the conal components. We analyze the single pulse polarization data of PSR B0329+54 at 606 MHz, and find that in its conal components, one sense of circular polarization dominates in the leading component while the other sense dominates in the trailing component. Our simulation shows that changing the sign of the impact parameter changes the sense of circular polarization as well as the swing of polarization angle.

*Subject headings:* Radiation mechanism; Rotation; Stokes parameters; Pulsars

## 1. Introduction

Although a lot of effort has been devoted for understanding the pulsar radiation mechanism, it seems, we still do not have a unified model for the emission mechanism and the beam structure. Three major models have been proposed to explain the coherent radio emission from pulsars: emission by bunches (e.g., Komesaroff 1970; Sturrock 1971; Tadamaru 1971; Ruderman and Sutherland 1975; Buschauer and Benford 1976, 1980; Michel 1978), relativistic plasma emission (e.g., Melrose and Gedalin 1999; Asseo and Riazuelo 2000) and maser

---

<sup>1</sup>E-mail: peyman@iiap.ernet.in

<sup>2</sup>E-mail: ganga@iiap.ernet.in

mechanisms (e.g., Yiyan et al. 1994; Malov and Chugunov 1995). Most of them make use of a secondary pair plasma and place the origin of the pulsar radiation at the inner region of the magnetosphere. However, the polarization observations (e.g., Clark and Smith 1969; Blaskiewicz et al. 1991) tend to favor the curvature radiation as the emission mechanism. But, the coherent curvature emission by bunches has been criticized (e.g., Melrose 1981) for its failure to explain the creation and stability of bunches.

The rotation vector model (RVM) by Radhakrishnan and Cook (1969) has been used to interpret the average polarization angle swing; it assumes a strong dipole magnetic field and collimated relativistic flow of plasma. The emitted radiation is then polarized along or orthogonal to the curvature of the magnetic field and significantly polarized.

Manchester et al. (1975) and Stinebring et al. (1984 a&b) have discussed polarization characteristics of single pulses and found them highly polarized, with generally the linear polarization dominating over the circular polarization. They noted that the circular polarization sense reversal appears to occur close to the center of the sub-pulse. This signature is not frequency dependent, contrary to the predictions of propagation or plasma emission processes (Gangadhara et al. 1999; Gangadhara and Krishan 1993, 1995). Rankin (1983) has studied Stokes parameters for a sample of pulsars, and showed that the circular polarization patterns are not symmetric, specially for core dominant pulsars. Further, Radhakrishnan and Rankin (1990), in their phenomenological study of the polarization properties of pulsars, clarified two extreme types of circular polarization signature in the average profiles: (a) an anti-symmetric type wherein the circular polarization changes sense in mid pulse, and (b) a symmetric type wherein it is predominantly of one sense. They found a strong correlation between the sense of position angle swing and change in circular polarization sense.

Rankin (1983) suggested that core and conal emissions have different emission mechanisms, with circular polarization being a property of core emission only. Lyne and Manchester (1988) suggested that a gradual change in emission characteristics from the core region to the outer edge of the emission beam can accommodate observations better than two distinct emission processes. Han et al. (1998) have studied the circular polarization in pulsar integrated profiles, and found that the circular polarization is stronger in the central or 'core' regions of the pulses, but it is not confined only to this region as Rankin (1983) claimed.

Although the theoretical understanding of the polarization properties of pulsar radiation is a fascinating subject, the complexity of the details has eluded a major breakthrough so far. It seems impossible to accommodate all the diverse properties of the polarization within a single radiation mechanism. Gil and Snakowski (1990) have attempted to examine the polarization properties of the curvature radiation without taking into account the role of rotation. Gangadhara (1996) has estimated the energy of particles moving along rotating

magnetic fields but has not estimated the polarization of the emitted radiation. Blaskiewicz et al. (1991) have developed a model by taking into account the effect of rotation on the particle motion. They have assumed a constant emission height and estimated the effect of rotation only on the position angle swing.

In this paper, we further develop the mechanism of the curvature emission by including the rotation and coherency effects, and estimating the polarization parameters of the emitted radiation. In this treatment, we relax the assumption of a fixed emission height made by Blaskiewicz et al. (1991). We show, instead that the major observed features of the circular polarization can be explained by considering the emission from extended region. In Sec. 2 we introduce the equation of motion for individual particles and derive an expression for the radiation electric field. In Sec. 3 we estimate the Stokes parameters for coherent radiation electric field from bunches of plasma particles, by assuming that the bunches are in an instantaneous circular motion along the rotating magnetic field. In Sec. 4 we give the observational evidences in favor of predictions of our model.

## 2. Coherent Radiation from plasma

The curvature radiation from high energy plasma particles in a strong curved magnetic field is often postulated to be the mechanism for producing radiation in the pulsar magnetosphere. The equation for particle dynamics is given by

$$\frac{d\mathbf{p}}{dt} = q(\mathbf{E}_i + \frac{\mathbf{v}}{c} \times \mathbf{B}), \quad (1)$$

where  $\mathbf{E}_i$  is the electric field induced by the rotating magnetic field  $\mathbf{B}$  in the pulsar magnetosphere. The symbols  $q$ ,  $\mathbf{v}$ ,  $\mathbf{p}$  and  $c$  stand for particle charge, velocity, momentum and the speed of light, respectively. Goldreich and Julian (1969) have proposed that a beam of electrons (or ions) is accelerated at the polar cap by this electric field. Sturrock (1971) suggested that this accelerated particle beam will emit gamma rays by the curvature radiation. These high energy photons interact with the magnetic field and generate the electron–positron pairs. The pairs thus created are most likely to be in higher Landau levels, and therefore lose their perpendicular component of the momentum through the synchrotron radiation. The synchrotron photons with energies above 1 MeV can further decay into electron-positron pairs in the pulsar magnetic fields.

The coherent curvature radiation from these secondary plasma particles flowing along the curved magnetic field lines is one of the important mechanisms proposed to explain the very high brightness temperature ( $10^{25} - 10^{30}$  K) from pulsars (Pacini and Rees 1970; Sturrock 1971). If  $\mathbf{J}$  is the current density due to the flow of such a plasma then the Fourier

components of coherent radiation electric field are given by (Jackson 1962)

$$\mathbf{E}(\omega) = -i \frac{\omega e^{i\frac{\omega R}{c}}}{\sqrt{2\pi R c^2}} \int_{-\infty}^{+\infty} dt \int \hat{n} \times (\hat{n} \times \mathbf{J}) e^{i\omega(t - \frac{\hat{n} \cdot \mathbf{r}}{c})} d^3 \mathbf{r}, \quad (2)$$

where  $R$  is the distance between the observer and the emission point and  $\hat{n}$  is the unit vector representing the line-of-sight.

Consider a stationary Cartesian coordinate system  $xyz$ , as shown in Fig. 1, centered on the neutron star where  $z$ -axis is aligned with the rotation axis  $\hat{\Omega}$ . Assume that  $\hat{n}$ , magnetic axis  $\hat{m}$  and  $\hat{\Omega}$  lie in the  $x-z$  plane at time  $t = 0$ . Consider a plasma column with elliptical cross section flowing along the rotating magnetic field lines. Let  $s_0$  be the length of plasma column, and  $\xi_0$  and  $\eta_0$  be the major and minor axes of its elliptical cross section, respectively. Let  $\zeta$  be the angle between  $\hat{\Omega}$  and  $\hat{n}$ , and  $\zeta_c$  be the angle between  $\hat{\Omega}$  and the center of momentum (CM) velocity of plasma particles  $\hat{v}_c$ . The observer receives radiation when the angle between  $\hat{n}$  and  $\hat{v}_c$  is  $\leq 1/\gamma$ , where  $\gamma$  is the Lorentz factor of the plasma bunch. The phase  $\Omega t$  represents the instantaneous position of the magnetic axis  $\hat{m}$ . The instantaneous plane of the CM orbit of a bunch is assumed to be an arc of a circle which makes an angle  $\theta$  with the line-of-sight  $\hat{n}$ .

In the co-moving frame  $x'y'z'$ , plasma waves  $(\omega'_p, k'_p)$  are excited in the plasma column by the plasma instabilities such as the oscillating-two-stream instability (Ruderman and Sutherland 1975). Since plasma waves are longitudinal, they are capable of creating density fluctuations, which can behave like particle bunches. Let  $\rho$  be the instantaneous radius of curvature of the trajectory of particles in the CM plane and  $\mu$  be the angle along the arc of the trajectory measured with respect to  $y'$  axis which is used in the volume integration appeared in Eq. (2), and  $\hat{e}_\mu$  the unit vector tangent to the trajectory. In the co-moving frame the current density and the charge density are given by

$$\mathbf{J}' = \hat{x}' J'_0 \sin(k'_p x' - \omega'_p t'), \quad \sigma' = \sigma'_p \sin(k'_p x' - \omega'_p t'). \quad (3)$$

Using the Lorentz transformation, we transform the current density and charge density into rest frame  $i$ , and substitute  $\mathbf{J}$  into Eq. (2). Next by integrating it, we obtain

$$\mathbf{E}(\omega) = -i \frac{\omega e^{i\omega R/c}}{\sqrt{2\pi R c^2}} \mathbf{A}, \quad (4)$$

and

$$\mathbf{A} = \frac{J_0 N s_0 \xi_0 \eta_0}{2i} \frac{\sin[(k - k_p)s_0/2]}{(k - k_p)s_0/2} \frac{\sin(k\eta_0\theta/2)}{k\eta_0\theta/2} \left\{ \hat{e}\theta \left( \frac{6\rho^2}{\omega c^2} \right)^{1/3} L_1(z) - \hat{y} \left( \frac{36\rho}{\omega^2 c} \right)^{1/3} L_2(z) \right\}, \quad (5)$$

where  $\hat{\epsilon} = \hat{n} \times \hat{y}'$ , and  $(\omega, k)$  are the radiation frequency and wave number, and

$$\frac{\omega'_p}{\omega_L} = \frac{\kappa\gamma}{6} + \frac{1}{2\gamma}, \quad (6)$$

and the constant  $\kappa$  is of the order  $10^{-3}$  (Buschauer and Benford 1976). The parameter

$$z = \left( \frac{6\omega^2\rho^2}{c^2} \right)^{1/3} \left[ \frac{1}{2\gamma^2} + \frac{\theta^2}{2} - \frac{\omega'_p}{\gamma\omega} - \frac{\xi_0}{\rho} \right], \quad (7)$$

and for positive  $z$ , we have

$$L_1(z) = \frac{2}{3}z^{1/2}K_{\frac{1}{3}}[2(z/3)^{3/2}], \quad (8)$$

$$L_2(z) = i\frac{2}{3^{3/2}}zK_{\frac{2}{3}}[2(z/3)^{3/2}]. \quad (9)$$

The functions  $K_{\frac{1}{3}}$  and  $K_{\frac{2}{3}}$  are the modified Bessel functions.

## 2.1. Calculation of $\rho$ and $\theta$

In the previous section we derived an expression for the Fourier components of the radiation electric field  $\mathbf{E}(\omega)$  as a function of the radius of curvature  $\rho$  and the angle  $\theta$ . Now, we shall introduce a method to estimate these quantities in the  $xyz$  frame as functions of observable quantities such as  $\zeta$ ,  $\Omega t$  and the magnetic axis inclination angle  $\alpha$ . The angular width of open field line region above the polar cap varies as  $w = (r\Omega/c)^{1/2} = (r/R_{LC})^{1/2}$ , where  $R_{LC}$  and  $r$  are the light cylinder radius and emission height, respectively. These are the field lines, from which the coherent radio waves are expected to be produced. Blaskiewicz et al. (1991) have showed that, in the first order of calculations, the terms of the order of  $w^2$  are negligible in the equation of motion (Eq. 1).

We relax the assumption of confining the emission region to a constant radius made by Blaskiewicz et al. (1991), and calculate velocity and acceleration in the CM frame of particles along the portion of magnetic field lines from which the radiation is receivable. At an arbitrary time  $t$ , the magnetic axis can be represented as

$$\hat{m} = \sin \alpha [\hat{x} \cos(\Omega t) + \hat{y} \sin(\Omega t)] + \hat{z} \cos \alpha. \quad (10)$$

In a co-rotating magnetosphere, the guiding center velocity of the center of momentum is

$$\mathbf{v}_c \cong v_{\parallel} \hat{b} + \boldsymbol{\Omega} \times \mathbf{r}, \quad (11)$$

where  $v_{\parallel}$  is the velocity of the center of momentum parallel to  $\hat{b}$ , the unit vector tangent to the dipolar magnetic field lines (Hibschman and Arons 2001).

The condition for receiving the radiation is that line-of-sight should lie inside the particle radiation beam with angular width  $2/\gamma$ , which is met when  $\zeta_c \simeq \zeta$ . This helps us to write  $\hat{v}_c$  as

$$\hat{v}_c = \sin \zeta \cos \phi \hat{x} + \sin \zeta \sin \phi \hat{y} + \cos \zeta \hat{z} \quad (12)$$

Since  $|\hat{v}_c - \hat{m}|$ ,  $|\hat{v}_c - \hat{r}|$  and  $|\hat{m} - \hat{r}|$  lie inside the open field line region and all are, of the order of  $w$ . Therefore, we have

$$\hat{r} = \frac{2}{3} \left( \hat{v}_c - \frac{r}{c} \boldsymbol{\Omega} \times \hat{v}_c \right) \left( 1 + \frac{\epsilon^2}{18} \right) + \frac{1}{3} \left( 1 + \frac{2\epsilon^2}{9} \right) \hat{m} + O(w^3), \quad (13)$$

where

$$\epsilon = [\sigma^2 + 2 \sin \alpha \sin \zeta \{1 - \cos(\Omega t - \phi)\}]^{1/2}, \quad (14)$$

$\sigma = \zeta - \alpha$  is the impact parameter and  $\phi$  is the angle between  $\mathbf{v}_c$  and  $\hat{n}$ . Substituting this result for  $\hat{r}$  into Eq. (11) gives the center of momentum velocity  $\mathbf{v}_c$ . Differentiating  $\mathbf{v}_c$  with respect to time gives the acceleration

$$\mathbf{a} = -\frac{1}{2r} [\hat{m} c^2 - \hat{v}_c (\hat{v}_c \cdot \hat{m}) c^2 - 3cr \Omega (\hat{z} \times \hat{v}_c)] + O(w^3). \quad (15)$$

The instantaneous radius of curvature of a particle orbit is given by

$$\rho = \frac{v_c^2}{a} \cong \frac{2r}{[\epsilon^2 - (6r\Omega/c) \sin \alpha \sin \zeta \sin(\Omega t - \phi)]^{1/2}}. \quad (16)$$

The angle  $\theta$  between the line-of-sight and the instantaneous plane of orbit is given by

$$\sin \theta = \hat{n} \cdot (\hat{v}_c \times \hat{a}) \quad (17)$$

or

$$\begin{aligned} |\mathbf{a}| \sin \theta &= \sin \zeta [\sin \zeta \sin \phi \cos \alpha - \cos \zeta \sin \alpha \sin(\Omega t)] \\ &+ \sin \zeta \cos \zeta [\sin \alpha \cos \phi \sin(\Omega t) - \sin \alpha \sin \phi \cos(\Omega t)] \\ &- 3r\Omega \cos \beta \sin^2 \beta [1 - \cos(\Omega t)]/c, \end{aligned} \quad (18)$$

where  $|\mathbf{a}|$  is the magnitude of acceleration. Equations (16) and (18) specify  $\rho$  and  $\theta$  as functions of pulse phase. Substituting these relations into Eq. (2) gives  $\mathbf{E}(\omega)$  as a function of the rotation phase. From Eqs. (16) and (18) we infer that:

a) If  $\rho_l$  is the curvature of particle trajectory on the leading side ( $\Omega t - \phi < 0$ ) and  $\rho_t$  is the curvature on the trailing side ( $\Omega t - \phi > 0$ ) then Eq. (16) shows that  $\rho_l < \rho_t$ .

b) For phases  $\pm\phi$  on either sides of the orbital plane, which is at  $\phi = 0$ , Eq. (18) shows that  $\theta$  is asymmetric, i.e., the values of  $\theta$  are not same at  $\pm\phi$ .

## 2.2. Stokes parameters

Let  $E_y(\omega)$  and  $E_\epsilon(\omega)$  be the components of radiation electric field  $\mathbf{E}(\omega)$  given by Eq. (4). Then the Stokes parameters can be defined as

$$\begin{aligned} I &= E_y E_y^* + E_\epsilon E_\epsilon^* \\ &= W^2 D^2 S^2 \left\{ \frac{4}{27} \left( \frac{36\rho}{\omega^2 c} \right)^{2/3} z^2 K_{\frac{2}{3}}[2(z/3)^{3/2}]^2 + \theta^2 \left( \frac{6\rho^2}{\omega c^2} \right)^{2/3} \left( \frac{4}{9} \right) z K_{\frac{1}{3}}[2(z/3)^{3/2}]^2 \right\}, \end{aligned} \quad (19)$$

$$\begin{aligned} Q &= E_y E_y^* - E_\epsilon E_\epsilon^* \\ &= W^2 D^2 S^2 \left\{ \frac{4}{27} \left( \frac{36\rho}{\omega^2 c} \right)^{2/3} z^2 K_{\frac{2}{3}}[2(z/3)^{3/2}]^2 - \theta^2 \left( \frac{6\rho^2}{\omega c^2} \right)^{2/3} \left( \frac{4}{9} \right) z K_{\frac{1}{3}}[2(z/3)^{3/2}]^2 \right\}, \end{aligned} \quad (20)$$

$$U = 2 \operatorname{Re}(E_y E_\epsilon^*) = 0, \quad (21)$$

$$\begin{aligned} V &= 2 \operatorname{Im}(E_y E_\epsilon^*) \\ &= -2W^2 D^2 S^2 \left( \frac{36\rho}{\omega^2 c} \right)^{1/3} \left( \frac{6\rho^2}{\omega c^2} \right)^{1/3} \left( \frac{4}{3^{5/2}} \right) \theta z^{3/2} K_{\frac{2}{3}}[2(z/3)^{3/2}] K_{\frac{1}{3}}[2(z/3)^{3/2}], \end{aligned} \quad (22)$$

where

$$W = \frac{J_0 N_0 S_0 \xi_0 \eta_0}{2}, \quad D = \frac{\sin(k\eta_0\theta/2)}{k\eta_0\theta/2}, \quad S = \frac{\sin[(k - k_p)s_0/2]}{(k - k_p)s_0/2}, \quad (23)$$

where  $N_0$  is the number of radiating bunches in a column. The polarization position angle is defined as

$$\psi = \frac{1}{2} \tan^{-1} \left( \frac{U}{Q} \right). \quad (24)$$

Since  $U$  is zero,  $\psi$  can be zero or  $\pi/2$ . However,  $\psi = \pi/2$  represents the real orientation of  $\mathbf{E}(\omega)$ , as predicted by Eq. (2). Note that due to the special choice of the coordinate system- $\hat{e}\hat{y}\hat{n}$  attached to the center of momentum,  $\psi$  becomes constant for a given field line. But when the line-of-sight moves from field line to field line due to rotation, polarization position angle swings in agreement with the rotation vector model (Radhakrishnan and Cook 1969). In the  $xyz$  coordinate system, the position angle is the angle between the radiation electric field and the projected spin axis on the plane of sky. Since the particle acceleration  $\mathbf{a}$  is parallel to  $\mathbf{E}$ , we shall use  $\mathbf{a}$  as the reference for convenience. Since  $\hat{n}$  is normal to both the plane of sky and  $\hat{y}$ , the plane of sky contains the  $y$ -axis. Hence the linear polarization angle  $\psi$  can be estimated from

$$\tan \psi = \frac{\hat{a} \cdot \hat{y}}{\hat{a} \cdot (\hat{n} \times \hat{y})}. \quad (25)$$

After substituting for  $\hat{a}$ , it can be simplified as

$$\psi = \tan^{-1} \left[ \frac{3 (r\Omega/c) \sin \zeta - \sin \alpha \sin(\Omega t)}{\sin \sigma + \sin \alpha \cos \zeta [1 - \cos(\Omega t)]} \right]. \quad (26)$$

### 3. Numerical calculation

For numerical calculations we adopt the values of emission heights and component locations provided recently by Gangadhara and Gupta (2001) for PSR B0329+54 at 606 MHz. Even though they have proposed nine emission components, we consider only three strong components marked as i, iii and iv in Fig. 4a, which have higher polarization. Out of these three, iii is a core component, and i and iv are the conal components of cone number 3 (Gangadhara and Gupta 2001). The phase locations of the components i and iv are  $-12.6^\circ \pm 0.64^\circ$  and  $9.5^\circ \pm 0.64^\circ$ , respectively. They assumed zero pulse phase for the core, however, the core is expected to be produced at some height above the polar cap and most likely shifted from zero pulse phase to the trailing side due to aberration and retardation. In our calculation we assume core component is emitted at an height of  $r_{\text{core}} \simeq 2r_{\text{NS}} \simeq 20$  km above the polar cap.

The dipole magnetic field strength of PSR B0329+54 is about  $B_0 = 1.2 \times 10^{12}$  G at the surface of the neutron star. Using the characteristic curvature radiation frequency given by  $\omega_c = (3/2)\gamma^3(c/\rho)$ , we can estimate the particle Lorentz factor,  $\gamma$ . For  $\nu_c = \omega_c/(2\pi) = 606$  MHz, emission height  $r_{\text{cone}} = 600 \pm 180$  km, Eq. (16) gives  $\rho_l \simeq 10^4 \pm 10^3$  km and  $\rho_t \simeq 2 \times 10^4 \pm 10^3$  km. For these values, we find  $\gamma = 300 \pm 190$  for leading component i and  $480 \pm 60$  for trailing component iv. Having the estimates of particles Lorentz factor, we compute the Stokes parameters using Eqs. (19)–(22).

Coherency factor  $S^2$  (Eq. 23) becomes maximum for  $k \simeq k_p$ , i.e., the coherency is more effective when the radiation wave number is of the order of the plasma wave number. We use this resonant matching condition in our numerical calculation of polarization parameters. The diffraction term  $D^2$  takes a maximum value  $\simeq 1$  for the parameters used in our calculations. Further, since radius of curvature is much greater than the plasma columns height  $\xi_0$ , the last term on the right hand side of Eq. (7) is negligible compared to the other terms.

Figure 2 shows the results of the numerical estimation of intensity I, linear polarization  $L = \sqrt{Q^2 + U^2}$ , circular polarization V and linear polarization angle  $\psi$ . To calculate the polarization of each component in this figure, we considered a bunch of field lines with a proper rotation phase. The main features of Fig. 2 are:

a) The asymmetry in the phase location of conal components i and iv with respect to the core iii arises due to the fact that the emission height of conal components is higher than the core component, which is explained as aberration and retardation effect by Gangadhara and Gupta (2001).

Since Blaskiewicz et al. (1991) considered the constant emission height they could estimate only the influence of aberration on the pulse width but not retardation. But we have relaxed the assumption of constant emission height by estimating the emission over the range of height, where the conditions are conducive for the coherent curvature emission. So, we are able to estimate the change in components width due to both the aberration and the retardation, which is almost double the value predicted by Blaskiewicz et al. (1991).

b) Figure 2a shows that the phase width of the component i is broader than that of the component iv. This broadening is a consequence  $\rho_l$  becoming smaller than  $\rho_t$ . We propose that this result can have observational evidences. In the next section we analyze the components width of 24 pulsars to check this prediction.

c) As we expected from our discussion on radius of curvature with similar particle densities on the field lines the Stokes parameter, I, for trailing component becomes stronger than that of the leading in agreement with Jackson(1962, Eq. 14.93).

d) We define the clockwise rotation of  $\mathbf{E}(\omega)$  as negative circular polarization ( $V < 0$ ) and counter clockwise rotation as positive circular polarization ( $V > 0$ ) then Fig. 2a shows that all the three components (i, iii and iv) display the well known anti-symmetric type of circular polarization. However, there is a difference in the relative magnitudes of circular polarization on either sides of each component center, i.e., positive V dominates over negative V in the case of component i while in component iv negative V dominates. This happens because of the fact that, due to the inclination of plane of field lines with respect to rotation axis, while observing say component i we tend to receive more radiation from the leading side of the plane of any given field line (associated with that component) compared to that received from the trailing side of the same field line.

In the case of core component the planes of magnetic field lines are nearly parallel to the rotation axis. Therefore we tend to receive equally both positive and negative parts of circular polarization from either sides of field line planes. Hence circular polarization becomes anti-symmetric for the core component.

Further the circular polarization is affected by rotation in such a way that in the case of leading component it makes positive V weaker but in the case of trailing component it enhances negative V. The simulated curve representing V in Fig. 2a depicts this behavior.

e) Figure 2b shows the polarization angle swing with respect to pulse phase. It shows that the centroid of polarization angle curve shifted toward the trailing side. This shift arises due to the rotation as proposed by Blaskiewicz et al. (1991). However, Hibschman and Arons (2001) have shown that current flow above the polar cap can shift polarization sweep in the opposite direction.

f) For the purpose of comparison we repeated the calculation of Stokes parameters by changing the impact parameter to  $-2.5^\circ$ , and plotted in Fig. 3b. We notice that the change of sense of impact parameter  $\sigma$ , flips the polarization angle swing and sense of circular polarization.

## 4. Observational evidences

Our model predicts that due to rotation the width of leading component becomes broader than the width of the trailing component. Further, the circular polarization on the leading component dominates with one sense while on the trailing component the other sense dominates. To find the observational evidences in this regard we analyzed the average profiles of about 24 pulsars and also the single pulse polarimetric data of PSR B0329+54.

### 4.1. Effect of the rotation on component width

We estimated the components width on trailing and leading sides of the average profiles of 24 pulsars using the data available in EPN format on web. We compared the full width at half maxima for leading component ( $\text{FWHM}_l$ ) and trailing component ( $\text{FWHM}_t$ ) of each pulsar. To select our sample we considered the following criteria: a) The pulse profile should not change drastically over the range of 600 MHz to 1000 MHz, i.e., the pulse profile should be stable through out this range of frequencies. b) The conal components should be prominent and not affected by the presence of core component. c) The leading and trailing components should be distinguishable enough, so that we can fit Gaussians to them without ambiguity.

According to Rankin’s (1990) classification the best candidates for our sample are conal Double, Triplet and Multiple pulsars. We choose 8 of the pulsars referred as Double conal in Rankin (1990), and not considered the sources like PSR B1133+16 because they may have more weaker components than the visible components in the average pulse profiles (Nowakowski 1996). We found the  $\text{FWHM}_l$  and  $\text{FWHM}_t$  by fitting Gaussians to the pulse components, and estimated their ratios. We did this analysis at different frequencies for each

Table 1. Pulse width comparison

| PSR B   | Frequency (MHz) | Period (s) | $\text{FWHM}_l/\text{FWHM}_t$ | Reference* |
|---------|-----------------|------------|-------------------------------|------------|
| 0052+51 | 610             | 2.115      | $1.032 \pm 2.20\text{E}-02$   | gl98       |
| 0059+65 | 610             | 1.679      | $1.052 \pm 2.22\text{E}-02$   | gl98       |
| 0148-06 | 610             | 1.465      | $1.136 \pm 7.49\text{E}-03$   | gl98       |
| 0226+70 | 610             | 1.467      | $1.3574 \pm 0.0$              | gl98       |
| 0301+19 | 610             | 1.388      | $0.937 \pm 0.0$               | gl98       |
| 0525+21 | 610             | 3.746      | $1.056 \pm 0.0$               | gl98       |
| 0559-05 | 610             | 0.396      | $1.772 \pm 0.0$               | gl98       |
| 0818-41 | 660             | 0.545      | $1.319 \pm 2.85\text{E}-02$   | qmlg95     |
| 0834+06 | 4800            | 1.274      | $0.868 \pm 2.0$               | kkwj97     |
| 1254-10 | 610             | 0.617      | $1.106 \pm 2.59\text{E}-02$   | gl98       |
| 1601-52 | 138             | 0.658      | $1.178 \pm 6.24$              | qmlg95     |
| 1648-17 | 606             | 0.973      | $1.190 \pm 0.0$               | gl98       |
| 1800-21 | 1642            | 0.134      | $0.850 \pm 3.58\text{E}-02$   | gl98       |
| 1822-09 | 610             | 0.769      | $1.141 \pm 0.0$               | gl98       |
| 1823-13 | 1642            | 0.101      | $1.190 \pm 9.98\text{E}-02$   | gl98       |
| 1839-04 | 606             | 1.840      | $1.442 \pm 9.10\text{E}-03$   | gl98       |
| 1914+09 | 610             | 0.270      | $1.628 \pm 0.0$               | gl98       |
| 1919+21 | 610             | 1.337      | $1.111 \pm 0.0$               | gl98       |
| 1935+25 | 606             | 0.201      | $0.839 \pm 0.0$               | gl98       |
| 1942-00 | 646             | 1.046      | $1.354 \pm 3.90$              | kmj96      |
| 2020+28 | 610             | 0.343      | $1.150 \pm 0.0$               | gl98       |
| 2044+15 | 610             | 1.138      | $1.572 \pm 1.45\text{E}-02$   | gl98       |
| 2053+21 | 606             | 0.815      | $0.920 \pm 0.0$               | gl98       |
| 2224+65 | 610             | 0.682      | $1.025 \pm 8.98\text{E}-03$   | gl98       |

\*gl98: Gould and Lyne (1998); kmj96: Kaspi et al. (1996); kkwj97: Kijak et al. (1997); qmlg95: Qiao et al. (1995)

pulsar and presented only the results at 610 MHz, except for a few sources for which the data was not available at this frequency. Table. 1 shows the sample and ratio of the FWHM of leading to trailing components for a set of 24 pulsars. It shows that 19 out of 24 pulsars have broader leading components than trailing one. Of course, for sources like PSR B0834+06 most likely a core component exists close to the trailing component and consequently it is broader than the leading component.

We performed Kolmogorov–Smirnov test on the two data sets comprising of one for the leading side components width, and the other for trailing side components width. The mean component widths were  $5.83^\circ$  and  $5.06^\circ$  for the leading and the trailing components, respectively. The Kolmogorov–Smirnov statistic D was found to be  $0.17^\circ$ , and the significance level P was  $0.86^\circ$ . The 95% confidence interval for the actual mean widths were  $3.24^\circ$  and  $2.71^\circ$  for the leading and trailing components, respectively.

#### 4.2. Interpretation of circular polarization from PSR B0329+54

To study the nature of circular polarization from PSR B0329+54, we analyzed the single pulse data at 606 MHz taken on August 30, 1996 from the Lovell telescope at Jodrell Bank. We considered about 2500 single pulses with time resolution of 0.249 ms. The average polarization parameters: intensity I, linear L and circular V polarization are plotted as functions of pulse phase in Fig. 4a. The continuous line curve indicates I while the broken and dotted ones represent L and V, respectively, in arbitrary units. The average polarization angle (bullet symbols) is given in Fig. 4b.

The gray-scale maps in Fig. 4b-d show the frequency of occurrence of polarization parameters with respect to the pulse phase in single pulses. We used the *pgplot* routines developed by Pearson (1989) for making gray-scale maps. The Fortran subroutine *pggray* draws gray-scale map of an array of the polarization parameters vs phase, by determining the shade of each point from the corresponding array value. The shade is a number in the range from 0 to 1 obtained by *linear interpolation* between the background level (white) and the foreground level (black). The white regions in the maps are with shade = 0 and darkest regions are with shade = 1. This technique has become a powerful tool in analyzing the pulsar polarization properties (e.g. Stinebring et al. 1984a,b). The panels (b), (c) and (d) in Fig. 4 represent the polarization angle, linear and circular polarization gray-scale maps, respectively.

The darkest shades represent the most probable regions of occurrence. The gray-scale maps were made from all those phase bins where the linear polarization L is above  $4\sigma$  level.

Here  $\sigma$  is the *rms* of  $L$  in the off pulse region. All those phase bins, where the condition  $L^2 + V^2 \leq I^2$  was not met, were excluded as they lead to spurious polarization quantities.

The average circular polarization was obtained from the gray-scale map (Fig. 4d) and the continues curve superposed in Fig. 4d. Note that for the sake of plotting on the selected scale, the whole curve has been amplified by a factor of 5. It shows under the leading component it is positive and negative under the trailing component while it is anti-symmetric under the core. This type circular polarization can be explained by considering the dipolar magnetic field lines with inclined magnetic axis with respect to the rotation axis. In agreement with this observational result, our Fig. 2a shows the dominance of positive circular polarization under the leading component and negative dominance under the trailing component, and anti-symmetric type under the core.

## 5. Conclusion

We have calculated the Stokes parameters  $I$ ,  $Q$ ,  $V$  for pulsars radio emission by taking into account the effect of the neutron star's spin for the first time. Figures 2a and 3a shows that under the influence of rotation, intensity  $I$  for the leading component becomes less than that of the trailing component for a similar distribution of emitting particles on different field lines.

According to the conal model (Rankin 1983a,b, 1990, 1993) the emission regions on the polar cap are organized in concentric hollow cones. Our simulation shows that the leading component becomes broader than its trailing counterpart. This broadening is induced by rotation through change in curvature of particle trajectories, as discussed in section 3. By analyzing 24 pulsar pulse profiles we find that 19 of them have leading components broader compared to trailing ones, and thereby confirm the possibility of detecting such an effect through observations. We note that such a broadening becomes observable only when the emission components are organized in the form of nested cones.

We have found, due to the inclination of magnetic axis with respect to the rotation axis and alteration of the particles trajectory by rotation, one sense of circular polarization becomes stronger in conal components of single pulses. Due to this enhancement of one sense of circular polarization in single pulses, one sense of circular polarization survives in the conal components of average pulse profile. It is worth mentioning that the inclination of magnetic field planes with respect to the line-of-sight is mainly responsible for the enhancement of one sense of circular polarization in conal component. But in the case of core component this effect vanishes and consequently lead to the circular polarization with an anti-symmetric

profile.

Radhakrishnan and Rankin (1990) found a strong correlation between the senses of polarization angle swing and circular polarization. Our simulation shows that changing the sign of impact parameter flips the sense of circular polarization and polarization angle swing. Therefore, the above correlation is caused by change in the sign of the impact parameter. The centroid of polarization angle curve does not coincide with the pulse center as a consequence of rotation.

We thank Y. Gupta and V. Krishan for carefully reading the manuscript and making comments. Also, we are grateful to A. G. Lyne for providing the Jodrell Bank data of PSR B0329+54. Part of this research has made use of the EPN data base maintained by the Max-Planck Institut für Radio Astronomie on web.

## REFERENCES

- Asseo, E. and Riazuelo, A. 2000, MNRAS, 318, 983
- Blaskiewicz, M., Cordes, J.M. and Wasserman, I. 1991, ApJ, 370, 643
- Buschauer, R., and Benfold, G. 1976, MNRAS, 177, 109
- Buschauer, R., and Benfold, G. 1980, MNRAS, 190, 945
- Clark, R.R., and Smith, F.G. 1969, Nat., 221, 724
- Dirac, P. A.M. 1938, Proc.Roy.Soc.London, A, 167, 148
- Gangadhara, R.T. and Krishan, V. 1993, ApJ, 415, 505
- Gangadhara, R.T. and Krishan, V. 1995, ApJ, 440, 116
- Gangadhara, R.T., Lesch, H., and Krishan, V. 1999, MNRAS, 307, 830
- Gangadhara, R.T. 1996, A&A, 314, 853
- Gangadhara, R.T., and Gupta, Y. 2001, ApJ, 555, 31
- Gil, J.A., and Snakowski, J.K. 1990, A&A, 234, 237
- Goldreich, P., and Julian, W.H. 1969, ApJ, 157, 869
- Gould, D. M., and Lyne, A.G. 1998, MNRAS, 301, 235

- Hibschman, J. A., and Arons, J. 2001, *ApJ*, 546, 382
- Han, J.L, Manchester, R.N., Xu, X.A., and Qiao, J.G. 1998, *MNRAS*, 300, 373
- Jackson, J.D., 1962, *Classical Electrodynamics*, Jhon Wiley and Sons, Inc. New York, p. 676
- Kaspi, V.M., Johnston, S., Manchester, R.N., Stairs, I., Crawford, F.Lyne, A.G., and D’Amico, N. 1996, *AJ*, 111, 2028
- Kijak, J., Kramer, M., Wielebinski, R., and Jessner, A. 1997, *A&A*, 318, L63
- Komesaroff, M.M. 1970, *Nat.*, 225, 612
- Lyne, A.G., and Manchester, R.N. 1988, *MNRAS*, 234, 477
- Malov, D.E., Chugunov, and Yu. V.i. 1995, *Astron. Reports*, 39, 625
- Manchester, R.N., Taylor, J.H., and Huguenin, G.R. 1975, *ApJ*, 196, 83
- Melrose, D.B., and Gedalin, M.E. 1999, *ApJ*, 521, 351
- Melrose, D.B. 1981, in Sieber W., Wielebinski R., eds, *Pulsar, 13 years of Research on Neutron Stars*. D. Reidel: Dordrecht, p.133
- Michel, F.C. 1978, *ApJ*, 220, 1101
- Pearson, T.J. 1989, *PGPLOT Graphics Subroutine Library*, Caltech, Pasadena, A-18
- Qiao, G.J., Manchester, R.N., Lyne, A.G., and Gould, D.M. 1995, *MNRAS*, 274, 572
- Radhakrishnan, V., and Cooke, D.J. 1969, *ApJLet.*, 3, 225
- Radhakrishnan, V., and Rankin, J.M. 1990, *ApJ*, 352, 258
- Rankin, J.M., 1983, *ApJ*, 274, 333
- Ruderman, M.A., and Sutherland, P.G. 1975, *ApJ*, 196, 51
- Stinebring, D.R., et al. 1984a, *ApJSS*, 55, 247
- Stinebring, D.R., et al. 1984b, *ApJSS*, 55, 279
- Sturrock, P.A. 1971, *ApJ*, 164, 529
- Tademaru, E. 1971, *APSS.*, 12, 193

Yihan, Z., Dingyi, M., Deyu, W, and Xinji, W. 1994, A&A, 282, 467

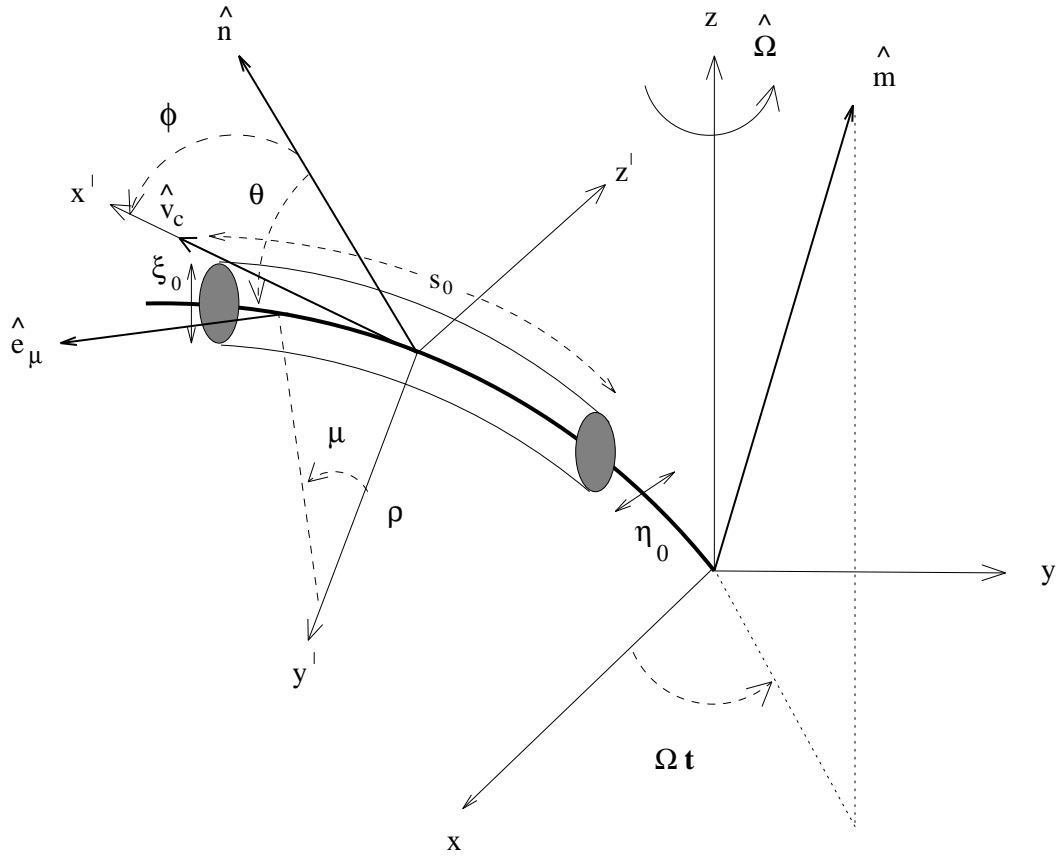


Fig. 1.— Emission region geometry. The lab frame  $xyz$  centered on the neutron star and  $x'y'z'$  is the co-moving reference frame. The column of plasma with length  $s_0$  and elliptical cross section with major axis  $\xi_0$  and minor axis  $\eta_0$  contains  $N_0$  bunches of coherently radiating particles.  $\hat{n}$  and  $\hat{m}$  are the line of sight and magnetic dipole unit vectors.

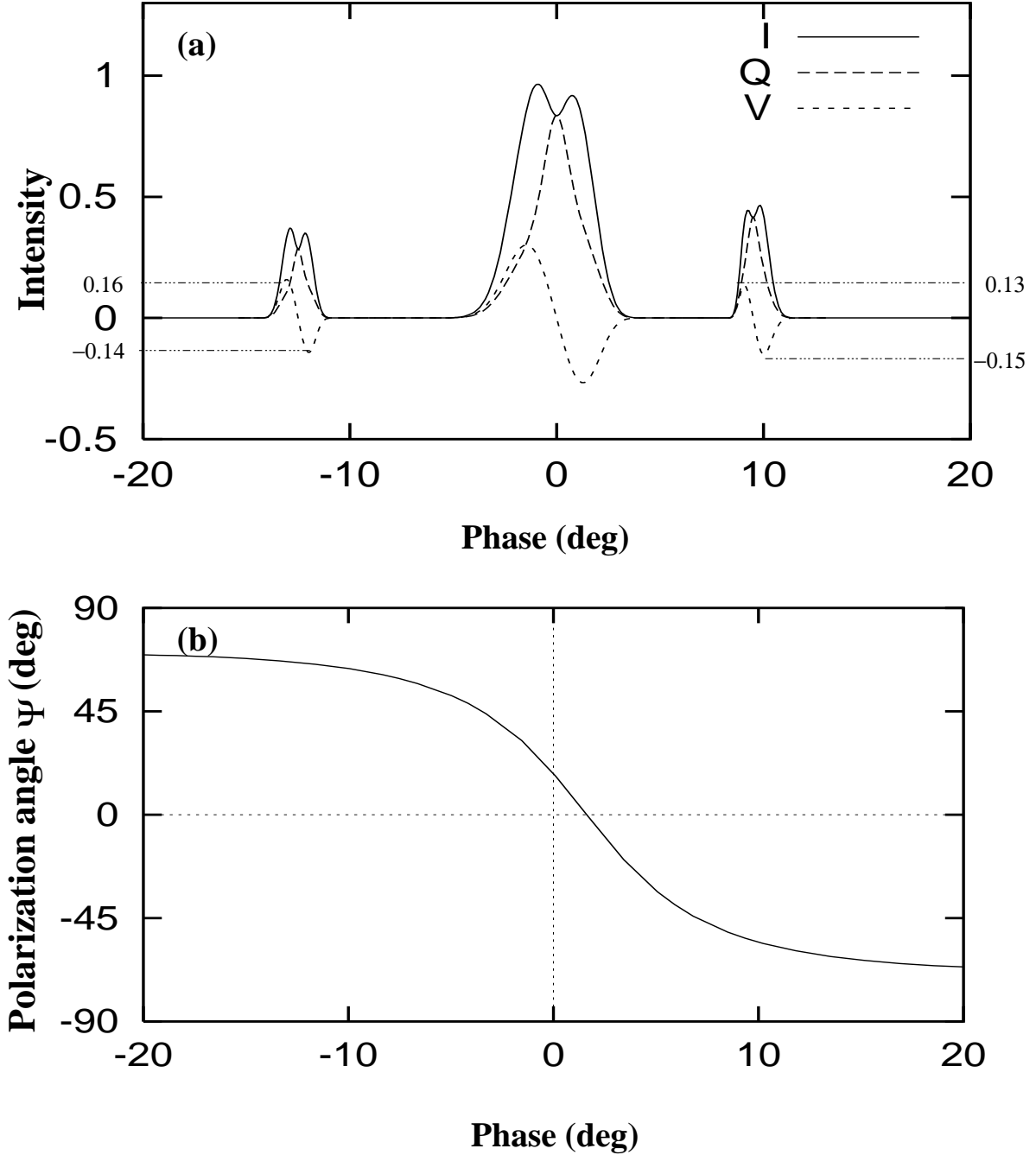


Fig. 2.— (a) Normalized Stokes parameters, I, L, V, and (b) polarization angle for a single pulse simulated using  $\alpha = 30^\circ$ ,  $\sigma = 2.5^\circ$ ,  $\omega_L = \omega_r/3$  and  $\omega_r = 610$  MHz.

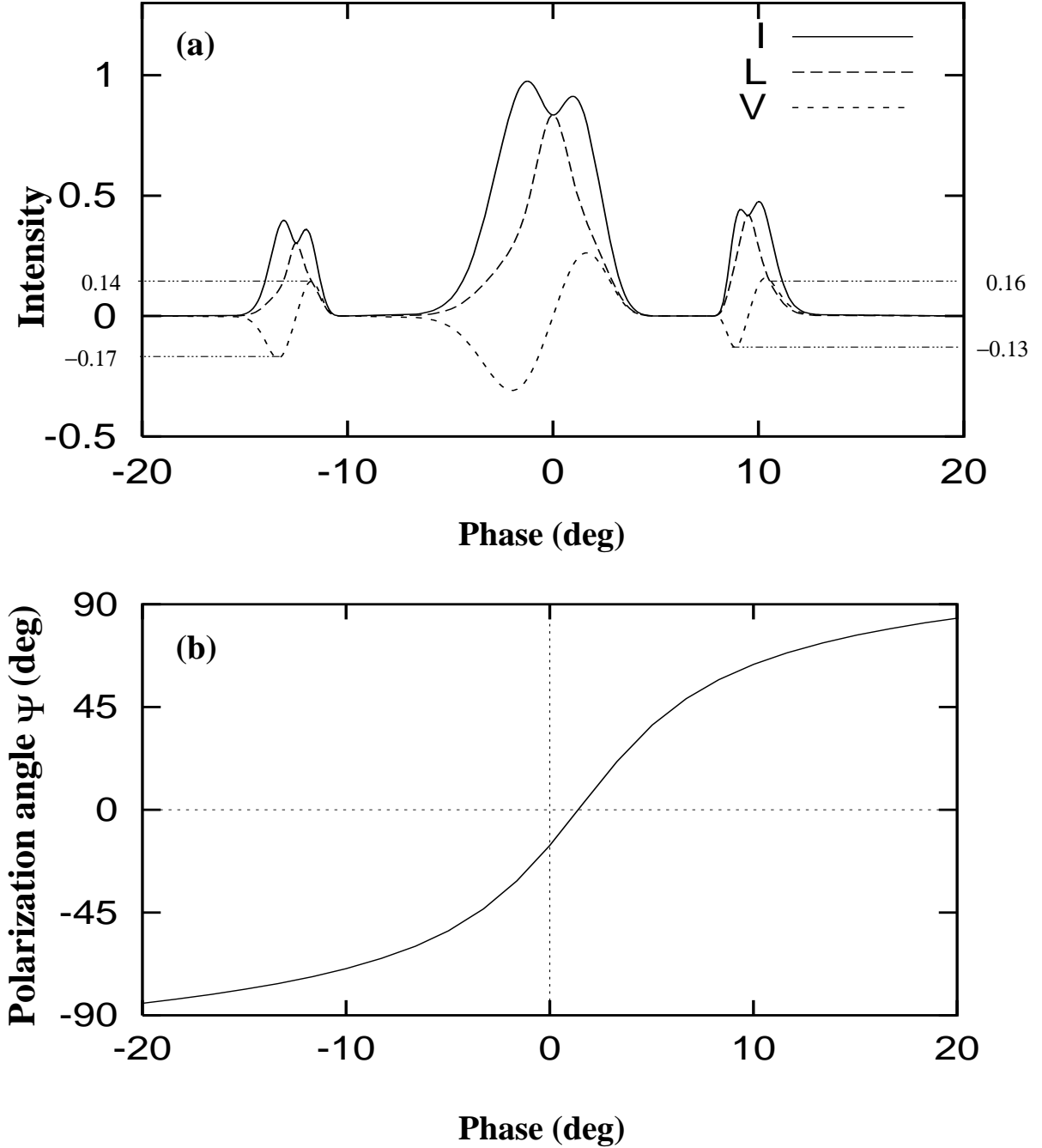


Fig. 3.— (a) Normalized Stokes parameters,  $I$ ,  $L$ ,  $V$ , and (b) polarization angle for a single pulse simulated using  $\alpha = 30^\circ$ ,  $\sigma = -2.5^\circ$ ,  $\omega_L = \omega_r/3$  and  $\omega_r = 610$  MHz.

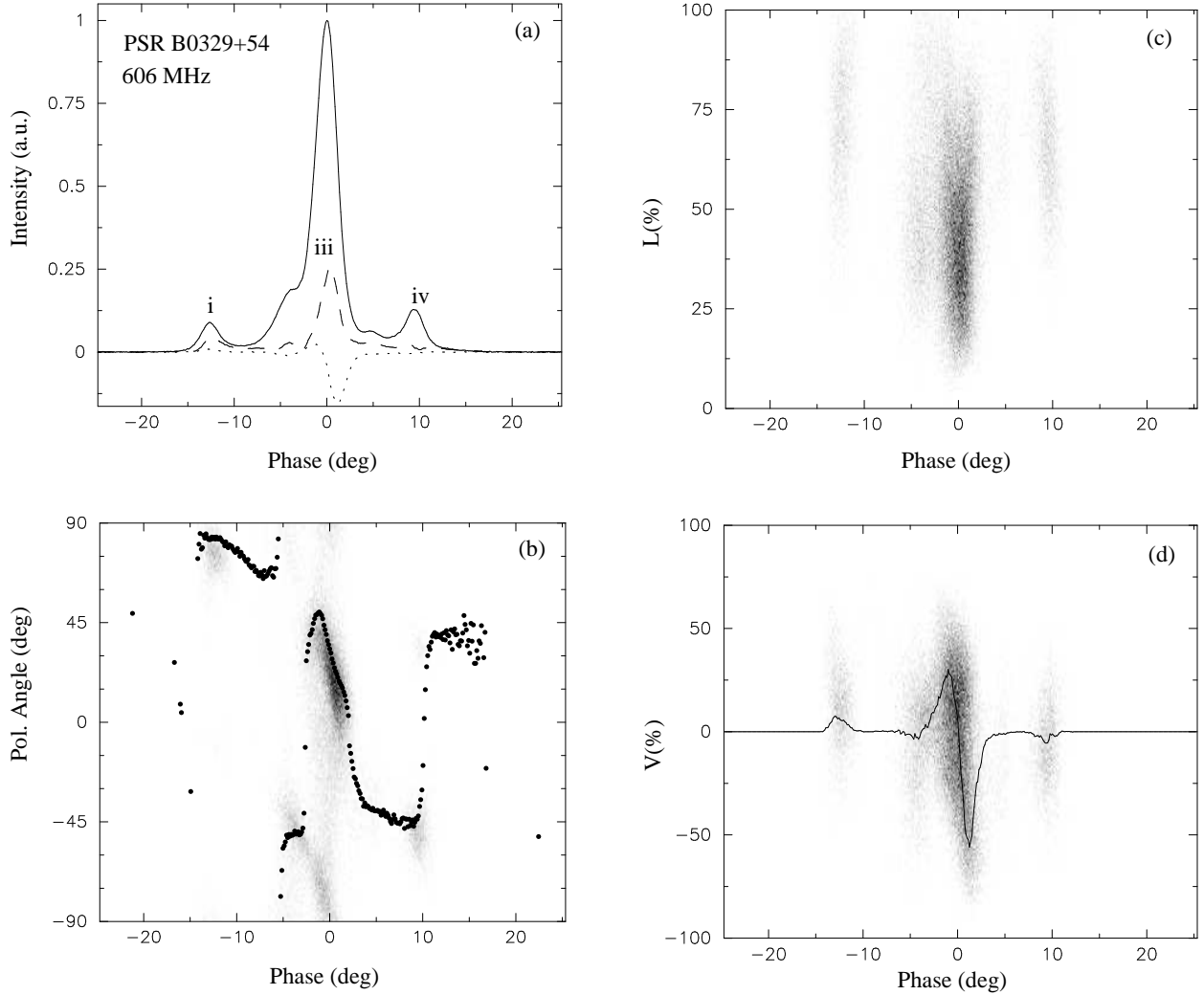


Fig. 4.— (a) The average pulse profile of PSR B0329+54 with arbitrary intensity units (a.u), and (b) average polarization angle ( $\psi$ ) (bullet symbols), and polarization angle gray-scale map obtained from individual pulses. The panels (c) and (d) represent the gray-scale maps of  $L(\%)$  and  $V(\%)$ . The shade is a number in the range 0 (white) and 1 (black) obtained by linear interpolation between the background and foreground levels. The average circular polarization curve (solid line) is superposed in the panel (d).